Hydrophobicity Classification of RTV Silicone Rubber-Coated Insulators Using Deep Learning Algorithms

by

Farook Abdalla Hussein Mustafa

A thesis

presented to the University of Waterloo

in fulfillment of the

thesis requirement for the degree of

Master of Applied Science

in

Electrical & Computer Engineering

Waterloo, Ontario, Canada, 2022

Author's Declaration

I hereby declare that I am the sole author of this thesis. This is a true copy of the thesis, including any required final revisions, as accepted by my examiners.

I understand that my thesis may be made electronically available to the public.

Abstract

Silicone rubber-based outdoor polymeric insulators are widely employed in electric power transmission and distribution networks to replace the conventional ceramic insulators, owing to their superior performance in contaminated and wet environments. Silicone rubber (SIR) insulators offer several advantages like high hydrophobicity, low cost, vandalism resistance and light weight. However, when exposed to electrical (dry band arcing and partial discharge) and environmental stresses (humidity, ultraviolet radiation, acid rain and pollution) they suffer from different forms of aging. The first form of aging is the temporal loss of hydrophobicity. However, SIR insulators can recover the hydrophobicity property due to the diffusion of the low molecular weight (LMW) from the bulk of the insulating material to the insulators' surface. Hence, it is important to classify the hydrophobicity status of SIR insulators as an indication of the aging degree. Different methods have been implemented to classify the hydrophobicity of the insulator surface including static contact angle measurement, dynamic contact angle measurement and hydrophobicity class (HC). The later technique is the most practical method that can be used in the field and can assess wide surface area. The surface wetting tendency is manually classified using one of six classes, i.e. HC1-HC6, where HC1 refers to a completely hydrophobic surface and HC6 is a completely hydrophilic surface. The main objective of this thesis is to automatically assess the hydrophobicity classes of non-ceramic insulators under a variety of conditions using deep learning techniques. A dataset of hydrophobicity classes (HC1-HC6) was created and prepared including 4197 images each having 2242×24 pixels size to train the proposed model. Several deep learning techniques,

including Convolutional Neural Networks (CNN), Transfer Learning (TL), and Object Detection (OD), were used in this thesis to categorize and assess the hydrophobicity classes of ceramic insulator coated with room temperature vulcanized silicone rubber (RTV-SIR). MobileNet model was found to have the highest accuracy and less training time after comparing with other CNN pretrained models. This model was then trained and tested under several conditions, including indoor, bright, and dark lighting conditions, and achieved accuracy of 97.77%, 89.44%, and 95%, respectively. Moreover, the proposed model achieved a recognition rate of 96.11% when tested on a full-scale silicone rubber insulator. The developed model was then deployed as a web application for convenience in the assessment of hydrophobicity classes. The proposed model could be utilized to evaluate SIR insulators surface conditions in an effective and automatic way under different conditions.

Keywords: Object Detection, Silicone Rubber, Hydrophobicity Classification, Dataset, Deep learning, Image Processing, CNN, Transfer Learning.

Acknowledgements

First and foremost, I would like to thank and praise Allah for helping and guiding me through this work and giving me the patience and health necessary to complete my master's degree.

My deepest thanks and appreciation go out to my supervisor, Prof. Ayman El-Hag, for his patience, assistance, guidance, inspiration, support, great supervision, and above all, friendship. Special thanks to my parents, family, and friends for their help and support.

Table of Contents

List of Figures

List of Tables

x

Chapter 1

INTRODUCTION

This chapter will cover the background information, such as overhead lines, different types of insulators and their differences, aging, and degradation. Additionally, the previous study that the scholars have done as well as the objective of this thesis.

1.1 Background

1.1.1 Overhead Lines (OHL)

The electric power network is composed of three different parts: power generation, power transmission, and power distribution. Electric power transmission systems usually transport electrical energy from power generation to power distribution networks using overhead transmission conductors at system voltages greater than 33kV. On the other hand, power distribution networks distribute the power from the transmission system to the consumer using both overhead lines and underground cables. Hence, overhead lines carry most of the electrical energy in electric power network and are considered as a preferrable way of transmitting electrical energy than the underground cables because of their less cost, ease of installation and inspection, fault detection and localization. A typical overhead line is composed of a utility tower, aluminum conductors, insulators, and different accessories as depicted in Figure 1. Outdoor insulators play an important part in the operation of the power system as they mechanically hold the conductors and electrically insulate them from the grounded

tower. There are mainly two different types of outdoor insulators, i.e., ceramic, and

non-ceramic insulators [1].
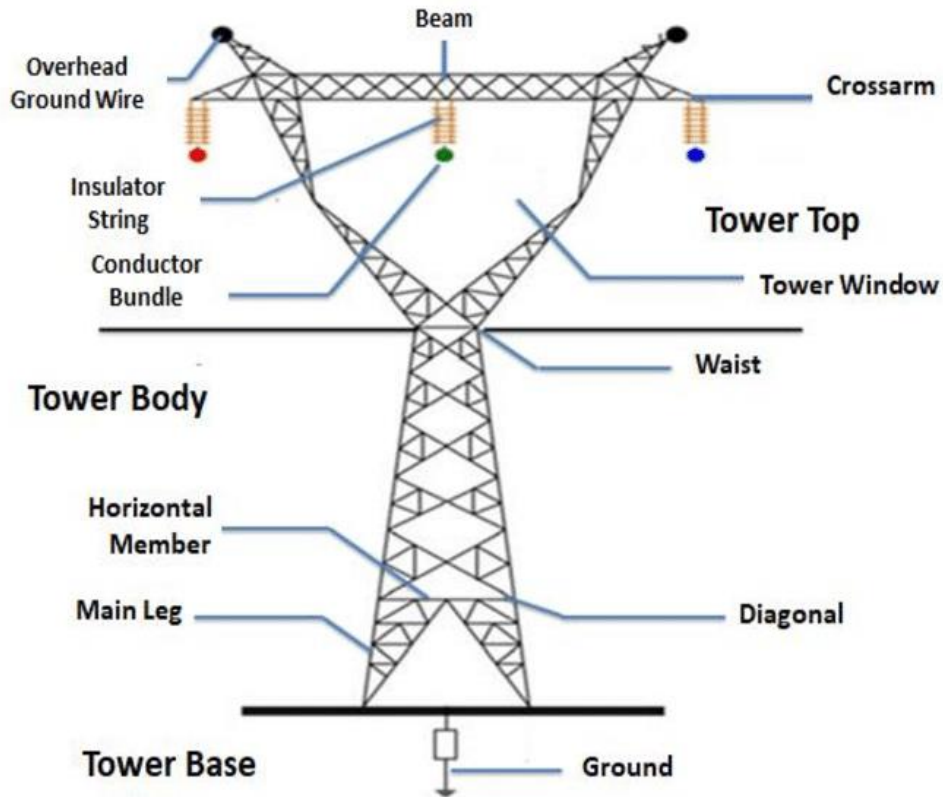
Figure 1. Typical overhead tower [2]

1.1.2 Ceramic Insulators

Ceramic insulators have been used in OHL for more than 100 years. Two main types

of ceramic insulators are typically used in OHL: cap and pin and long rod [3] as shown

in Figures 2 and 3 respectively. The traditional ceramic and porcelain insulators have

undergone numerous enhancements over the past few years in order to increase their

reliability, mechanical integrity, and long-term field performance [4]. For instance, as depicted in Figure 4, different profiles of ceramic insulators have been introduced that can be used at different pollution levels and types. However, ceramic insulators suffer from different disadvantages like a heavyweight, prone to breakage, and hydrophilic surface properties. The later property leads to the accumulation of pollution on the insulator's surface which can lead to the development of leakage current under humid conditions. If no remedy actions are taken, flashover is imminent leading to power flow interruption. Hence, different solutions have been proposed to improve the pollution performance of ceramic insulators including [6]:

- Regular washing
- Extending creepage distance
- Silicone grease coating on insulators
- Semi-conductive glaze insulators
- Application of coating on high voltage insulators

Figure 2. Ceramic Cap and Pin Insulators [3]

Figure 3. Insulators of the Long Rod Ceramic Type [3]

Regular washing is a procedure that can be used to ensure insulation performance in polluted environments, but two important factors must be considered, i.e., determining the best cleaning time interval and the financial cost, especially if live washing cannot be used [7]. While washing can be used to prevent flashover, it is a very costly solution, especially in highly polluted areas. Alternatively, creepage extenders were utilized to prevent pollution flashover. Each extender is sealed to the porcelain or glass insulators and adds 6" (150 mm) of creepage to the existing creepage distance of the insulator. This overall increase in the insulator creepage distance leads to lowering the electric stress and hence LC. Despite of its anti-contamination efficacy, the use of creepage extenders is limited because it is considered as an expensive solution and could increase the chances of partial discharge activities resulting from the distortion of electric field by utilizing different surface characteristics between the creepage extender and outdoor insulator [8]. Another approach to improve the pollution performance of ceramic insulators is changing their surface properties. For example, a semi-conductive glaze has been used that allows small current magnitudes to pass through its surface due to its semi-conductive properties, limiting the impact of fog and pollution accumulation and improving the distribution of electric field along the length of the insulator. However, because of its semi-conductive properties, the glaze may experience thermal runaway and power loss. Furthermore, using this technology on previously installed insulators is impractical.

Another modification to the ceramic insulator surface is the use of silicone grease coating (SGC). SGC decreases the possibility of flashover and excessive leakage currents by encapsulating the pollutant and hence minimizing the impact of pollution accumulation. However, there is a need for frequent removal of the old SGC which is expensive and time-consuming [8]. Alternatively, room temperature vulcanized (RTV) coating is applied to ceramic insulators. RTV coating prevents the formation of leakage current as it changes the surface property for ceramic insulators from hydrophilic to hydrophobic. However, due to aging and pollution accumulation, RTV coating may lose its superior hydrophobic properties. Nevertheless, RTV coatings can regain their lost hydrophobic properties due to the migration of low molecular weight (LMW) form the bulk of the material to the insulator surface. The lifetime for RTV coating is estimated to be 10-15 years before there is a need to reapply it.
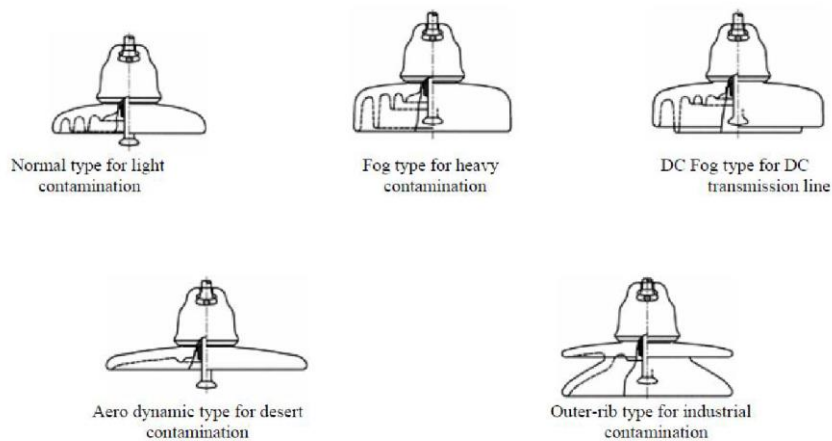
Figure 4. Different Disc Insulators [5]

1.1.3 Composite or Non-Ceramic Insulators (NCI)

Generally, a non-ceramic insulator (NCI) is made up of a fiber glass reinforced rod, a polymeric housing insulating material, and metallic end-fittings. The rod provides mechanical strength to the insulator which is bonded with a shed-shaped polymeric housing insulating material (silicone rubber (SIR), ethylene propylene diene monomer (EPDM)) [5]. A typical NCI is depicted in Figure 5.
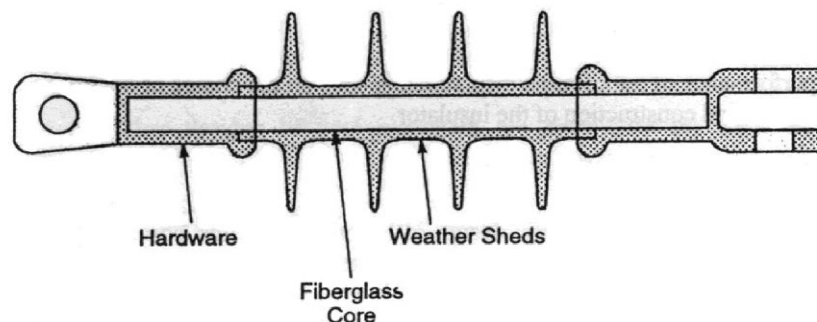
Figure 5. Insulator made of polymeric materials [5]

Non-ceramic insulators exhibit several advantages compared to ceramic insulators including lightweight, vandalism resistance, and hydrophobic surface properties due to low surface energy. However, various defects such as cracks, air voids, and impurities may be present in the GFR or polymeric material as a result of mishandling, aging, or manufacturing defects. Although the majority of serious flaws are identified during the installation phase, still some flaws are hard to identify. Under continuous mechanical and electrical loading conditions, these defects may progress and propagate over time leading to insulator failure. Aging is considered the main cause of non-ceramic

7

insulators failure and will be discussed in section 1.1.4. A summary of the main

differences between ceramic and non-ceramic insulators is shown in Table 1 [10].

Table 1. Ceramic Insulators vs. NCIs [10]

	FACTORS	CERAMIC	NCIs
1	Resistant to contamination flashover.	Low	High
2	Pollution and contamination	Significantly impacted	Performance slowly affected
3	Hydrophobicity	hydrophilic	hydrophobic
4	Self-cleaning capability	Because of the glazing and the sheds inclination	Due to recovery of hydrophobicity capability
5	Maintenance	Needs maintenance such as cleaning, washing, and greasing.	No maintenance is Normally required
6	Weight	High	10%-35% of the conventional ceramic insulator
7	Vandalism and breakage resistance	Breaks and shatters into piece due to vandalism	Non-breakable

1.1.4 Aging and Degradation of NCIs

Because of their organic nature, NCIs and RTV-coated insulators age with time. The

surface resistance of NCIs decreases with age, making the insulator surface more

susceptible to deposition of contamination and moisture which may reduce the

wettability of the insulator surface [11]. There are two influencing factors that can

remarkably accelerate the aging of NCIs. Starting from the electrical stress, which

includes leakage current (LC) and partial discharge (PD). These stresses typically occur as a result of the development of dry bands, deposition of severe pollution, humidity, and because of overvoltage stresses. Environmental stresses include heat, ultraviolet (UV), rain, wind, snow, acid rain, coastal salt, and degradation due to biological organisms [9]. The synergistic effect of these stresses results in surface roughness, cracking, erosion, chalking, tracking, loss of hydrophobicity and elasticity, together they contribute to a reduction in the mechanical and electrical strength of non-ceramic insulators [11]. When the outdoor environmental stresses are applied at the same time with electrical stress, it can cause the loss of LMW siloxanes as well as the depolymerization of the polymeric material due to either chain scission or oxidation.

- Leakage Current (LC)

Silicone rubber based polymeric insulators possess a high surface resistance and, therefore, low surface tension. Both of these features are required to prevent the formation of water films and hence limit LC development. In the presence of moisture, fog, or mist, when conductive pollution deposits on the surface, it generates conductive dry spots on the surface of the insulator [9]. This leads to surface discharges that gives rise to the creation of a water film, which may result in the development of LC. Due to the uneven distribution of LC density, certain spots will be subjected to more joule heating than others leading to the formation of scattered and random dry bands [11]. As a result, these dry bands extend to both high voltage and ground electrodes across

the insulator length leading to the development of dry band arcing [10]. This will lead to an increase in the insulator surface temperature resulting in thermal degradation.

- Partial Discharge (PD)

Partial discharge (PD) is one of the major type of electrical stress which is caused by an increase in the electric field because of the loss of hydrophobicity resulting from the formation of continuous water films on the surface. The enhancement of the electric field at the triple point is attributed to difference in the dielectric permittivity of the insulator (ε= 2-3), water (ε=80), and air (ε=1) [12]. When the electric field surpasses the inception voltage for air breakdown (30 kV/cm), PD activities may be started [6]. The heat energy dissipated by the continuous discharges deteriorates the insulator's surface, causing a temporary loss of hydrophobicity in those areas. Another source of surface PD is the insulator close proximity with sharp electrodes resulting from defective hardware. Both types of surface PDs cause temporary hydrophobicity loss because of de-polymerization resulting from the scission of polymer chains or the oxidation reactions. Nevertheless, once these discharges seize to exist, SIR may regain some or all of its hydrophobic properties [13]. Moreover, chain scission or oxidation triggered by PD activities yields acidic byproducts which results in the depletion of low molecular weight siloxane species. This induces chemical reactions which cause bond breakage in molecular chains of polymer material, resulting in silanol and carbonyl groups, the cyclic volatile silicone oligomers, and intermolecular forces in the polymer matrix. Such forces prevent the volatile silicone rubber oligomers from resurfacing.

10

This, in turn, will reduce the SIR's ability for hydrophobicity recovery [11]. The simultaneous application of stresses can cause complete degradation and hydrophobicity loss on SIR insulator surface.

- Environmental Stresses

Environmental conditions including UV, humidity and/or pollution can contribute to the aging of non-ceramic insulators acting alone or synergically with the electric stress. For example, UV components can cause the scission of C-H and Si-C bonds as opposed to Si-O (siloxane and main chain) bonds. Although main chain scission is unlikely, crosslinking events can occur if Si-C and C-H links are broken. As a result, LMW chains, particularly those with n = 3 to 15 repeat units, would increase or decrease. Byproducts such as hydrocarbons would also be produced [14]. Also, acid rain can significantly cause the erosion of the SIR which results in the degradation of the insulator surface. The surface becomes rough as a result of acid rain causing erosion and deterioration, thereby decreasing surface hydrophobicity. Moreover, pollution accumulation on the insulator surface is responsible for a significant reduction of the hydrophobicity classes depending on the type, size, and chemical structure of the pollution. Furthermore, mold growth in humid environments can also decrease the hydrophobic behavior of SIR leading to LC development [11]. Finally, humidity can contribute to the field enhancement at the insulator surface leading to the development of PD activities which result in destroying the surface hydrophobicity of the SIR insulator [15].

11

1.1.5 Degradation Consequences

As a result of electrical and environmental stresses, different forms of aging can take place at the insulator surface including discoloration, hydrophobicity loss, crazing, erosion, tracking, chalking, roughness, alligatoring, punctures, and corona cutting [13]. Discoloration and loss of hydrophobicity are frequently the first and most visible indications of aging. Then, based on the severity of the aging factors, several types of degeneration can be formed. Electrical discharges along with UV radiation on SIR surface typically give the insulators a toothed and whitish dusty appearance which is termed as chalking [8], which can be shown in Figure 6. Chalking causes insulator to absorb a significant amount of water and pollution, which speeds up the degradation of SIR insulator. Surface cracks on the insulators are caused by electrical stresses such as PD and arcing. Crazing [11] is a term used to describe cracks that are less than 0.1 mm deep, as shown in Figure 7 [8]. Alligatoring is an worst form of crazing in which the cracks depth surpasses 0.1 mm which may result in rod exposure. As previously discussed, continuous corona discharges, particularly near the metallic end fittings or because of the loose connection between the rod and polymer housing insulation, can cause corona cutting, which significantly cause the electrical and chemical degradation of the insulator [8], which is depicted in Figure 8. Because of the organic nature of the polymeric housing materials, they lose their wettability which cause the development of leakage current and eventually, the permanent tracking and erosion [9]. Tracking results from the surface discharge activities which is considered as more severe than

erosion because it appears on the surface in the form of carbonaceous conducting traces, whereas erosion is non-conductive and degrades at a slower rate as shown in Figure 9 [8].
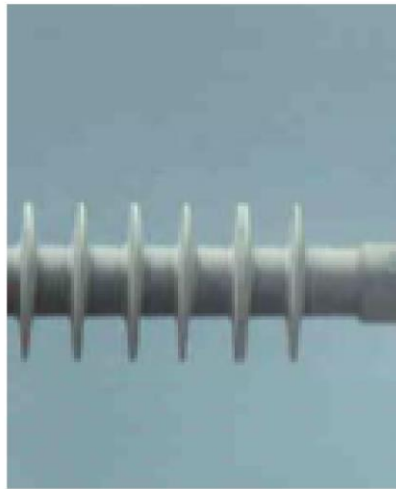
Figure 6. Chalking seen on non-ceramic insulators [8]

Figure 7. Crazing seen on non-ceramic insulators [8]

Figure 8. Corona Cutting [8]

a. [16]   b. [8]

Figure 9. Degradation of polymeric insulator due to the flow of LC: (a). Tracking and (b). Erosion.

1.2 Literature Review

1.2.1 Hydrophobicity Assessment

The degradation of a polymeric housing insulating material is often followed by the hydrophobicity loss of insulator. As previously stated, the surface hydrophobicity of an insulating material refers to its tendency to resist the water flow and resist the development

of continuous water channels on its surface. If an insulator surface is hydrophobic, water drops appear as a bead shape (independent water droplets) without flowing on the surface of the insulator. Such droplets have a contact angle greater than 90°. When the insulator's surface ages, the contact angle decreases until the surface becomes fully hydrophilic and the formation of water films. Figure 10 depicts the variation in hydrophobicity [8].

The contact angle is one technique for determining the hydrophobicity or hydrophobicity class (HC) of NCIs. Water droplets are injected with a syringe in this technique, and the contact angle (of the droplet) is measured on a flat surface. When the surface is tilted, the difference between the advancing and receding angles is measured, as shown in Figure 11 [20]. This method can only be applied when the insulator is not energized. and hence is not used in the field.
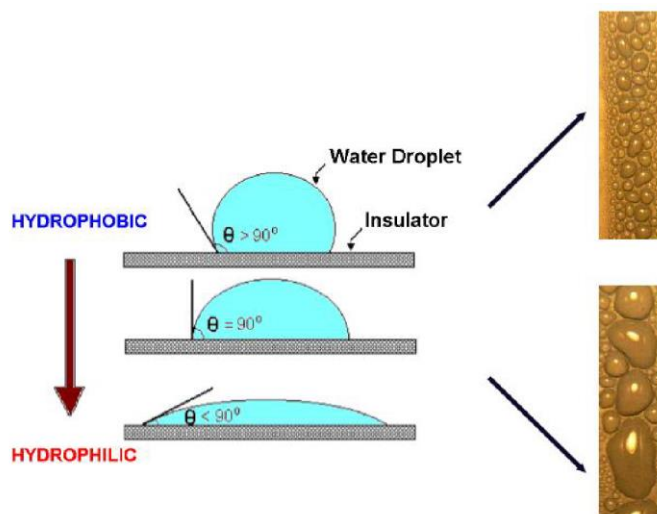
Figure 10. Surface of SIR insulator transitioning from Hydrophobic to Hydrophilic Conditions [8]
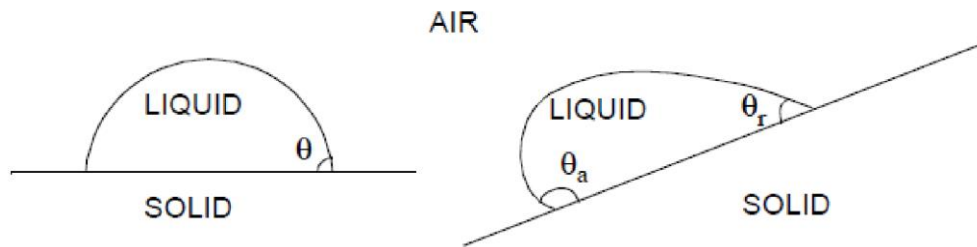
Figure 11. Contact Angle of water droplets with respect to Flat and Tilted Surfaces [20]

Another well-known measurement technique is the spraying of water in the form of mist on polymeric insulators is. As shown in Figure 12 [20], the wettability of the SIR surface is classified into seven classes starting from a fully hydrophobic surface (HC 1) to a fully hydrophilic surface (HC 7). These classes are evaluated based on the water drop contact angle, water drops pattern, and wetted surface area, as shown in Table 2 [20]. This technique is known as the STRI classification for hydrophobicity evaluation, which can also be used to comprehensively evaluate the aging condition and behavior of SIR insulator. The key disadvantage of this technique is it sole dependence on the judgment of the person conducting measurements.
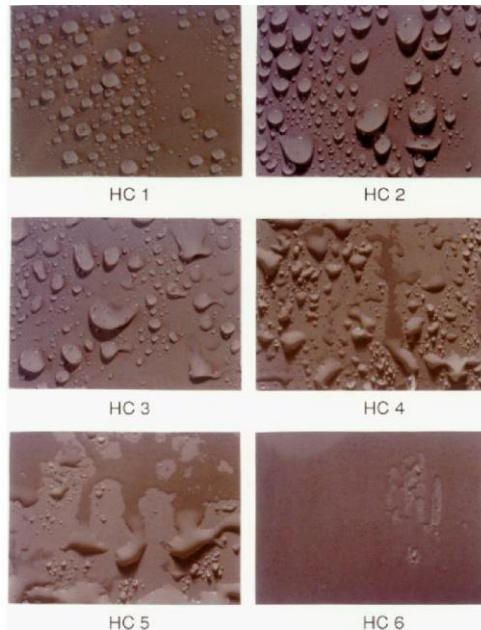
Figure 12. HC 1 to HC 6 [20]

Table 2. HC Evaluation Criteria [20]

HC	Description
1	It only forms distinct droplets. significantly larger for most of the droplets.
2	For the majority of droplets, only separate droplets form.
3	It only forms distinct droplets. for the vast majority of drops. Most of the time, they are no longer circular.
4	We see both individual droplets and wet traces left by the water runnels. Totally moist patches are less than 2 cm2. They collectively cover around 90% of the test area.
5	Over 2 cm2 of the test area have been totally wet, or about 90% of it.
6	Wetted areas cover more than 90% of the area; however, small un-wetted areas (spots/traces) are still visible.
7	The entire tested area was covered in a continuous water film.

Several attempts have been proposed using digital image processing (DIP) for the analysis and measurement of water drops contact angle, thereby determining HC and evaluating the insulator's condition to reduce human error. The hydrophobicity of polymeric insulators was calculated and evaluated using DIP in [21]. The proposed method employs human intervention in specifying the area containing the water droplets by removing the useless portions of the images. The classification can be done possible based on a ratio of the maximum water drops area divided by the total area of the image. To calculate the HC, it also takes into account the shape coefficient of the maximum water trace. Despite the efficacy of this method for online assessment of aging condition of insulator, it still depends on the user's intervention in identifying the region on the image and removing the background from the area selected on the image. Furthermore, the accuracy of this method is dependent on the user's skills while shooting the pictures, as well as the distance of the camera from the insulator surface.

Authors in [22] addressed the issue of human intervention by developing an algorithm for image processing based on extracting water drop pictures, then fitting the contours of the water drops by employing the orthogonal polynomial, and lastly determining the water drop contact angle for the evaluation of insulator's hydrophobicity. The major problem in this technique is that it is not applicable to the actual field conditions or the online evaluation of the insulator hydrophobicity. The researchers assumed that the water droplets contact angle should be limited to a change of 15° and that the water droplet should be at the center on the insulator surface, which does not always happen. Furthermore, the method evaluated the insulator using a single droplet instead of utilizing many droplets with varying size to simulate practical case.

18

This method can only be applied for localized assessment of the insulator surface and not the overall surface hydrophobicity evaluation. Other researchers [23-26] have utilized other DIP techniques to assess the hydrophobicity classes of the SIR insulators. These include circular factor, the Hough transformation, the scaled entropy, segmentation, the histogram analyses, textural analysis, surface energy, and fractal dimension were all used. While many researchers were unable to define a clear relationship with the hydrophobicity classification, others were able to develop a mathematical relationship to the Hydrophobicity classes of insulators. However, none of the attempts were successful in generalizing a classifier. The authors of [27] and [28] combined multiple features like shape and area in order to overcome the limitation of using only one feature. The use of the multiple features in order to assess the insulator's HC has eliminated the poor reliability associated with single-feature evaluation. Despite the fact that these techniques have improved recognition rates, they are still insufficient for determining the HC of the insulator under variable conditions. the success of these approaches depends on a specific configuration of fixed distance, light level, insulator position, and shape. To correctly classify the insulator in terms of HC, any changes to the experimental conditions requires a reconfiguration of the decision tree boundaries.

Attempts to automate this process using traditional machine learning (ML) techniques yielded high classification accuracy. Artificial neural networks (ANN) are extensively used compared to other intelligent approaches. The fact that NNs are very adaptive and learn fast is the key to accelerating their efficiency. The NN application methods can be divided into multiple approaches for various applications to produce effective testing results. According to [29] the

highest achieved accuracy was 96.5 percent when using ANN as a classifier and various image-based features such as grey level co-occurrence matrix (GLCM), Radon transform, contourlet transform, discrete cosine transforms (DCT), and discrete wavelet transforms (DWT). The authors of [30] and [31] employed the principle of probabilistic neural networks (PPN) as a classifier and several feature extraction techniques such as edge detection and GLCM. After extensive training, the maximum achieved accuracy was 95%. Using the multilayer perceptron (MLP) model described in [32], the authors achieved 93.8% recognition accuracy. In addition, for image processing, they used the grayscale conversion of the color image, local histogram transformation, and the Prewitt operator for edge detection. In [33] seven geometric metrics were extracted and utilized to evaluate the HC which are: number, mean eccentricity, water droplet coverage rate, coverage rate, perimeter, shape factor, and eccentricity of the greatest water droplet. The back propagation neural network (BPNN) was used as a classifier and achieved 96.6% accuracy. Principal component analysis (PCA) was used to reduce the number of features along with the adaptive neuro-fuzzy inference system (ANFIS) as a classifier in [34]. They found that the best features selected by PCA are average intensity, correlation, skewness, and homogeneity, with a classification accuracy of 94.85%. However, these techniques are time-consuming to employ because the user must manually specify which features to utilize while evaluating the images. Incorrect feature selection can result in unsatisfactory classification, which adds another source of human error.

Deep learning (DL) is being used instead of traditional ML algorithms as a new trend in the assessment of SIR. As shown in Figure 13, the difference between ML and DL approaches is

that DL does not require manual feature selection, making it easier to implement and less prone to incorrect feature selection. The authors of [35] employed DL techniques for HC and compared their results to those of [29] that used ML on the same dataset. It has been reported that using DL techniques achieved equivalent accuracy with the extra advantage of being easier to implement. Convolutional neural networks (CNN) were employed in [36, 37] to overcome the manual dependency on feature extraction for accurate detection of insulator wettability. CNN training time was reduced by using the transfer learning (TL) approach. Different CNN architectures were investigated such as VGG16, VGG19, GoogleNet, AlexNet, and ResNet. The performance of all the models was satisfactory, yielding very high recognition accuracy. As a result, the proposed methods can potentially be used in the field for remote condition monitoring of overhead line insulators. However, the aforementioned proposed methods have limited use because the training and testing occurred in controlled conditions.
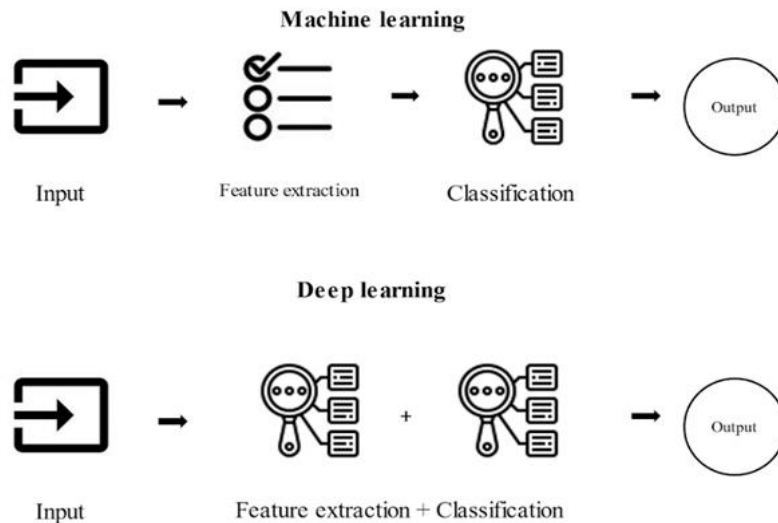
Figure 13. Difference Between Machine Learning and Deep Learning

1.3 Thesis Objectives and Problem Formulation

It is evident from the previous discussions, that there is currently no comprehensive approach for assessing the HC of SIR. Human intervention, localized evaluation, and specialized conditions hampered attempts to design an automatic robust system based on image processing. The goal of this thesis is to create a comprehensive system based on deep learning algorithms that can evaluate the condition of SIR insulators subjected to several conditions (insulator type, lighting conditions, distances, etc.) and without the need for human involvement. The Thesis specific goals can be summarized as follows:

- Aggregate and analyze 6 different classes of hydrophobicity evaluation data in different conditions.

- Leverage a deep learning model (MobileNet) in Python to predict the condition of the insulator.

- Enhance the model using object detection to improve the accuracy of the results.

- Develop and deploy the model as a web application to increase the usability of the project.

Chapter 2

MATERIALS AND METHODS

In this chapter, the collection and preparation of the dataset will be discussed. Also, the implemented methods and algorithms for HC will be explained.

2.1 The Dataset

Ceramic cap and pin insulator coated with room temperature vulcanized (RTV) high voltage coating were utilized to make the samples for this study. Images of classes 1–6 were obtained using the method proposed by [21]. The method suggests spraying the coated samples with distilled water and alcohol solutions. Various hydrophobicity classes (HC) can be created according to the quantity of alcohol by volume (ABV) in the distilled water solution, ranging from class 1 with 0% ABV to class 6 with 90% ABV. This is owing to the decreased RTV surface tension due to the increase of alcohol concentration. Such reduction in the surface tension will mimic the aging of the RTV surface. Figure 14 shows the obtained HC images with various ABV percentages.
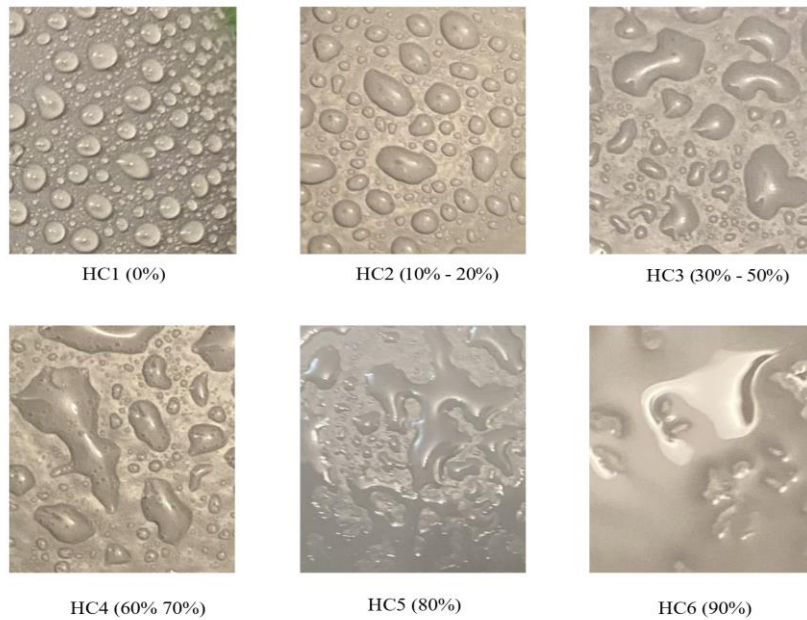
Figure 14. HC classes with various percentages of ABV solution

The original dataset contained a total of 2043 images, all of which were taken indoors and from various angles. The python library katna was used to crop each image to multiple different images to increase the dataset and provide enough training dataset for the DL algorithms. As a result, our dataset has increased to 4197 images. It is worth mentioning that only original RGB images were used in the training dataset without any alteration to their color. We split the dataset into three parts: training, validation, and testing, in the ratio of 80:10:10. Figure 15 shows the preprocessing step.

Original images

Cropped & resized images
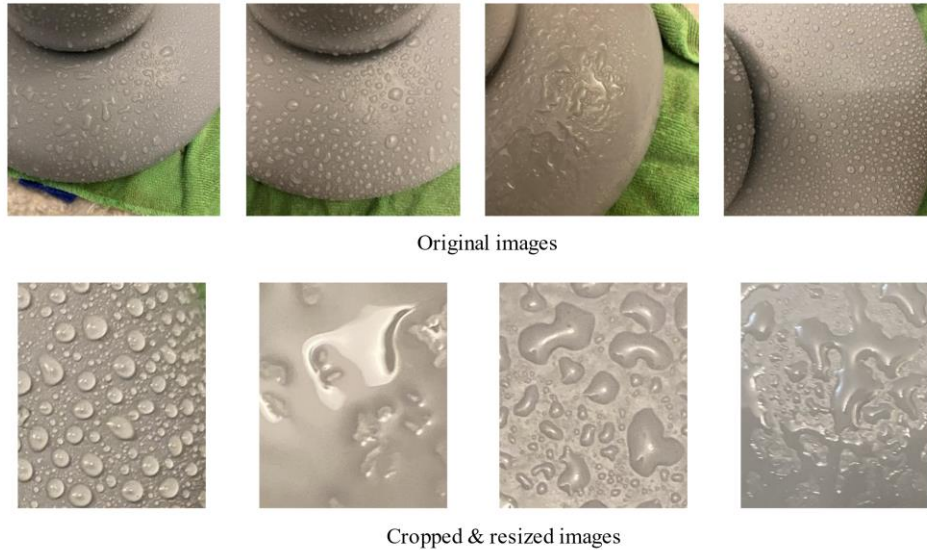
Figure 15. Preprocessing

2.2 Deep Learning Algorithm

One of the powerful deep-learning algorithms is convolutional neural network (CNN) which is broadly used in computer vision for extracting the features and perform classification of the images. As depicted in figure 16, the CNN is made up three layers, an input layer, many hidden layers, and fully connected output layers.

Convolutional layer: Firstly, the image inputted to this layer is processed by a number of filter banks which are called as kernels. In the forward paths, such filters are transversely convolved with the weight and height of the inputted image separately. It gives a two-dimensional (2-D) feature map for the detection of the pattern. Next, the rectified linear unit (ReLU) layer increases nonlinearity of the network by utilizing the rectified function [38].

25

Pooling layer: This layer is responsible for reducing the dimension of the feature map produced by the convolution layer while retaining the necessary and useful information. In addition, it also regulates data over-fitting via nonlinear down-sampling through various operators.

**Fully Connected Layer:** This layer is the output layer which provides the function of a classifier. This layer gives the network forward by converting the 2-D feature maps into a 1-D feature vector while calculating accuracy (scores) for each class. The SoftMax layer predicts the accurate class from the test dataset based on the trained model after converting the scores into probabilities.
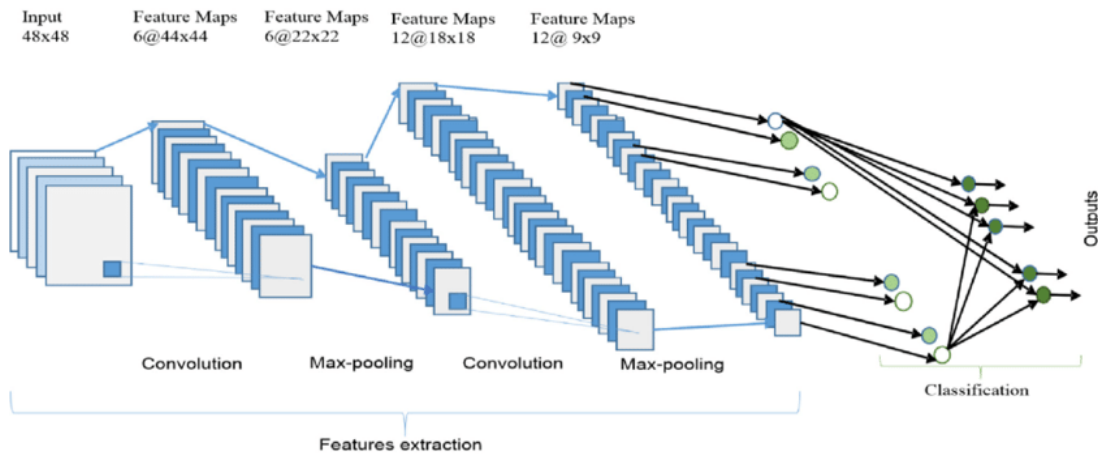
Figure 16. CNN architecture [39]

2.3 MobileNet

In this thesis we will use the MobileNets architecture proposed in [40], the MobileNets are a family of TensorFlow mobile-first computer vision models that are designed to maximize accuracy while keeping in mind the limited resources of an on-device or embedded application. MobileNet is a CNN class that is open sourced by Google, and it provides an ideal starting point for training using compact and quick classifiers. MobileNets are small, low-latency, low-power models that can be parameterized to meet the resource constraints of various cases. As shown in Figure 17, MobileNets can be used to build classification, detection, embeddings, and segmentation systems.
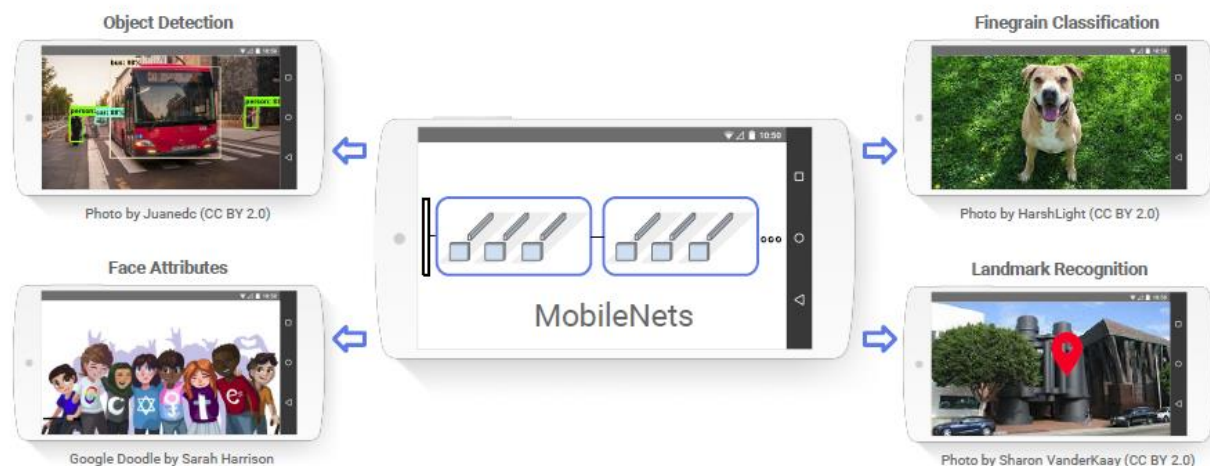
Figure 17. applications of MobileNets [40]

To understand the compactness of MobileNets, a brief comparison in terms of size and the number of parameters with one of the most well-known CNN architectures, VGG16, is provided. The full size of the VGG16 network is approximately 553 megabytes. On the other hand, the size of one of the largest MobileNets is only about 17 megabytes. This relatively low

size of MobileNets is important when considering deploying a model to a mobile app or running it in the browser. Table 3 shows the comparison between VGG16 and MobileNets in terms of size.

Table 3. Compares VGG16 to MobileNets in Terms of Size [40]

| Model	Size	Parameters
VGG16	553 MB	138,000,000
MobileNet	17 MB	4,200,000

MobileNet used depthwise separable convolutions to develop lightweight deep neural networks. When compared to the network with regular convolutions of the depth of the same nets, it significantly reduces the number of parameters. There are 28 layers in a MobileNet which can be reduced by appropriately tuning the width multiplier hyperparameter. The input image has a size of 224×224×3 and as depicted in figure 18, two operations are used to create a depthwise separable convolution:

- Depthwise convolution:

  The channel-wise $D_K \times D_K$ spatial convolution is depthwise convolution. If we have five channels in the figure below, we will have 5 $D_K \times D_K$ spatial convolutions.

- Pointwise convolution:

  The 1×1 convolution is used to change the dimension to pointwise convolution.
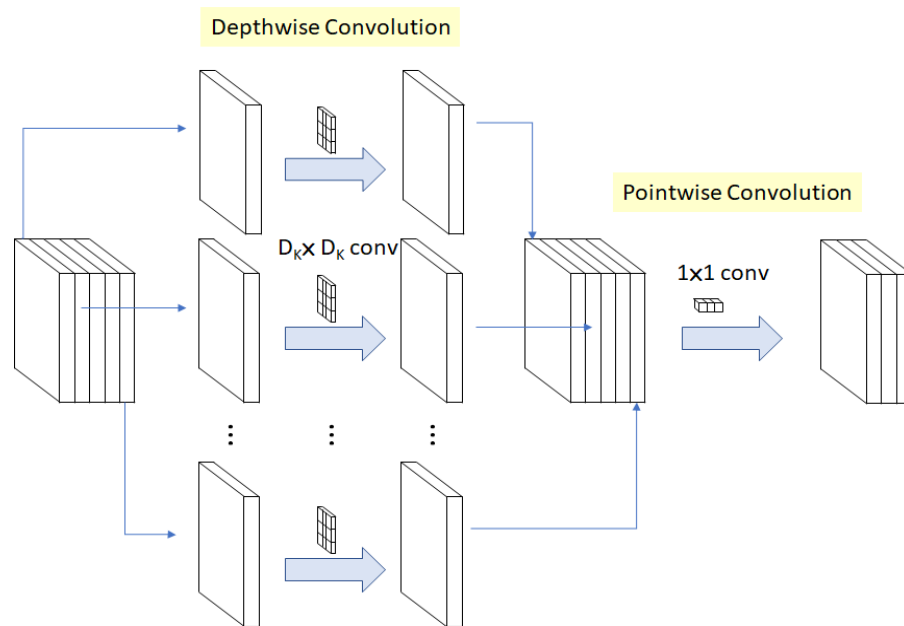
Figure 18. Convolution with Depth Separation [41]

The primary distinction between MobileNet architecture and traditional CNN architecture is that MobileNets divided the convolution into a 3x3 depth-wise conv and a 1x1 pointwise conv instead of a single 3x3 convolution layer followed by the batch norm and ReLU that is used in traditional CNN, as shown in Figure 19.
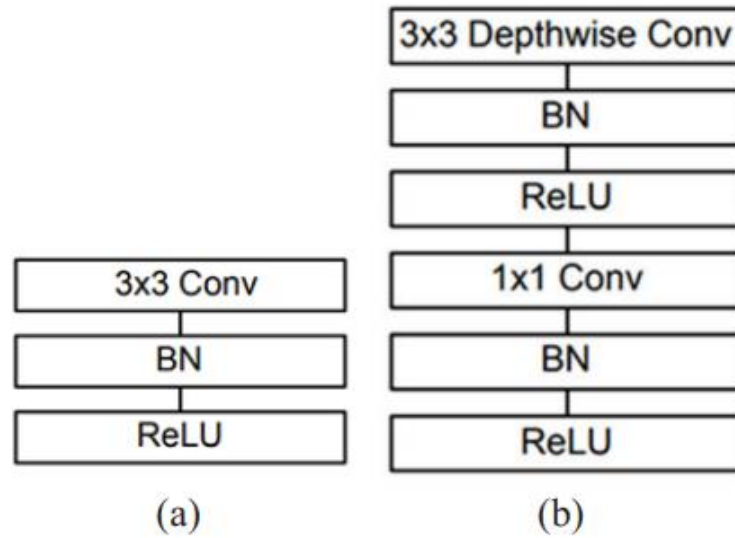
Figure 19. (a) Conventional convolutional layer with batch normalization and ReLU. (b) Depth-wise separable convolution with depth- and point-wise layers, then batch normalization and ReLU. [40]

2.4 Transfer Learning

The computation time required to train a network from scratch is an important issue in CNN. Another significant issue is the scarcity of insulator image data for HC classification. The transfer learning (TL) process is used to address these two issues. The weights of pre-trained models (MobileNet) that were not initially trained for HC are transferred to our model using TL. Only the last few hidden layers of the MobileNet pre-trained models (along with the classification layer) are replaced by the new layers of the HC classification problem with different weights and learning rates. So, instead of training the entire network from scratch with random weights, TL significantly reduces the network's training time, making it computationally faster and working reasonably well for small datasets [37]. The lower layers

30

provide traditional computer-vision feature extraction, such as edge detection, whereas the final layers focus on task-specific features. Furthermore, we can employ existing pre-trained models like VGG16 and AlexNet for previously untrained tasks like style transfer and face identification [42].
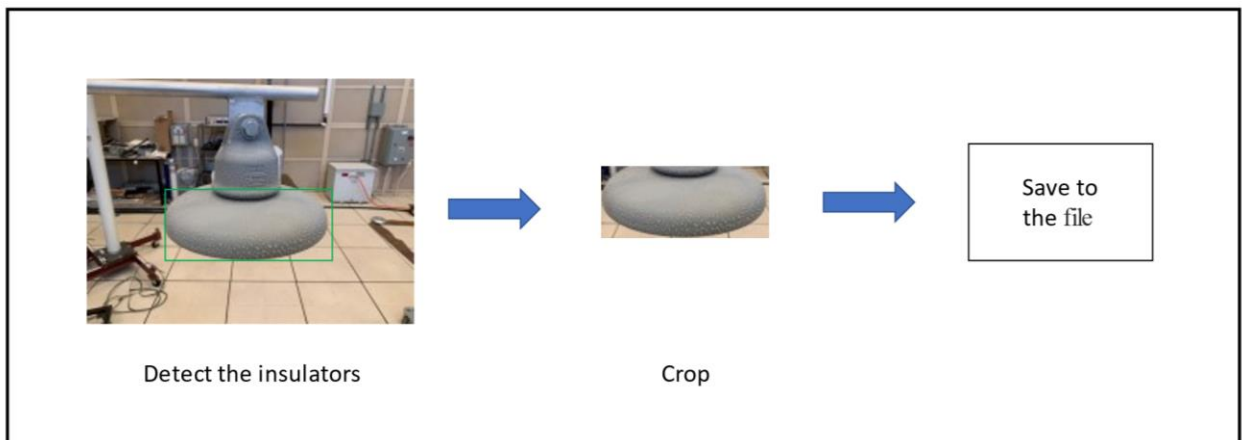
2.5 Object Detection

A problem that may occur during model testing is that the model may have selected the incorrect object, extracted incorrect features, or if there is any distraction in the original photo. To avoid this, we will use an object detection (OD) technique in this thesis. The OD is a computer technique linked to computer vision and image processing that detects instances of semantic items of a certain class (such as individuals, buildings, or vehicles) in digital photos and videos. Face detection and pedestrian detection are two well-studied object detection areas. The OD has various applications in computer vision, such as picture retrieval and video monitoring. There are several OD architectures; in this thesis, we will employ the Single Shot MultiBox Detector (SSD) proposed in [43]. The SSD architecture is a single convolution network that learns to anticipate and categorize bounding box locations in a single run. As a result, SSD may be trained from the beginning to the end. The SSD network is made up of a basic architecture (in this case, MobileNet) followed by numerous convolution layers. We just need one shot using SSD to recognize several objects inside an image, but RPN-based techniques such as the R-CNN series require two shots, one for generating region suggestions and one for recognizing the item of each proposal. As a result, SSD is substantially quicker than two-shot RPN-based techniques; The SSD architecture is depicted in Figure 20. The

TensorFlow object detection API provides a platform for building a deep learning network that can detect objects. They already have pre-trained models in their framework, which are called Model Zoo. Among the pre-trained models, MobileNet was used. As illustrated in Figure 21, we trained the OD model to detect insulators, crop them, and save them to a file for use as a testing dataset.
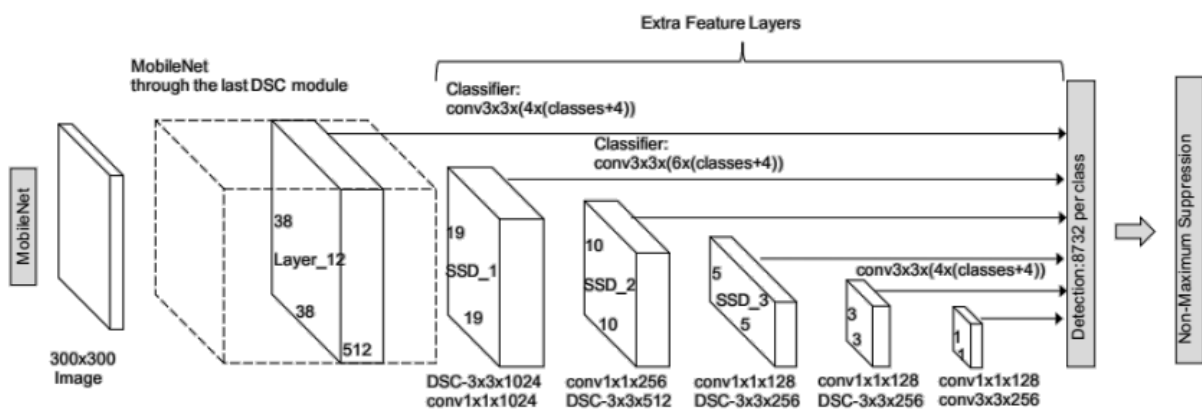
Figure 20. Layered SSD MobileNet Architecture [43]

Figure 21. Object Detection model steps

2.6 Model Deployment

Model deployment is essentially the engineering process of making a deep learning model available for real-world use. The deployment is frequently used interchangeably with making a model available via real-time APIs. It is also the process of integrating a machine learning model into an existing production environment in order to make realistic business decisions based on data. It is one of the final steps of the machine learning life cycle. Since one of our goals in this project is to utilize the proposed model in many conditions, one of which is to use the model in the field where technicians may find it difficult to run the code or use any programming languages. In this regard, we used the python package called Streamlit to deploy our model as a web application with a simple graphical user interface (GUI); Figure 22 shows the GUI for our project. In general, you can upload an image from your computer to the model, and it will predict the HC class as well as provide the probability of other classes. An example of the output of the GUI is shown in Figure 23.

Hydrophobicity Classification Prediction

This is a simple image classification web app to predict **Hydrophobicity Classes!**

Please upload an image file

Drag and drop file here
Limit 200MB per file • JPG, PNG, JPEG

Browse files

Please upload an image file

Figure 22. Graphical User Interface

It is a *HC1!*

Probability (0: HC1, 1: HC2, 2: HC3, 3: HC4, 4: HC5, 5: HC6

|	0	1	2	3
0	0.9999997615814209	1.3260614650789648e-7	9.14171707222522e-8	1.541387744550825

**Figure 23. GUI output**

Chapter 3

RESULTS AND DISCUSSIONS

3.1 Comparison between different CNN architectures

Different pre-trained CNN models were tested for the classification of hydrophobicity, which includes VGGNet16, MobileNet, MobileNetV2, and AlexNet. Initially, all the models were trained using the original dataset without any image processing and hence only raw RGB images were fed to the models for the training. We split the dataset into three parts: training, validation, and testing, distributed in a ratio of 80:10:10, respectively. Out of 2043 images, 1635 images were used for training, 204 images for testing, and 204 images for validation. The parameters for the models were selected for training purposes for optimized performance. The learning rate was chosen to be 0.001, the maximum epoch (iterations) was set to 50, and the batch size was set to 10. The training accuracy vs the epoch is shown in Figure 24. It is apparent that both the MobileNet and MobileNetv2 had the best training performance among all models in terms of training time, which was expected given that these two networks have smaller number of parameters compared to other models.
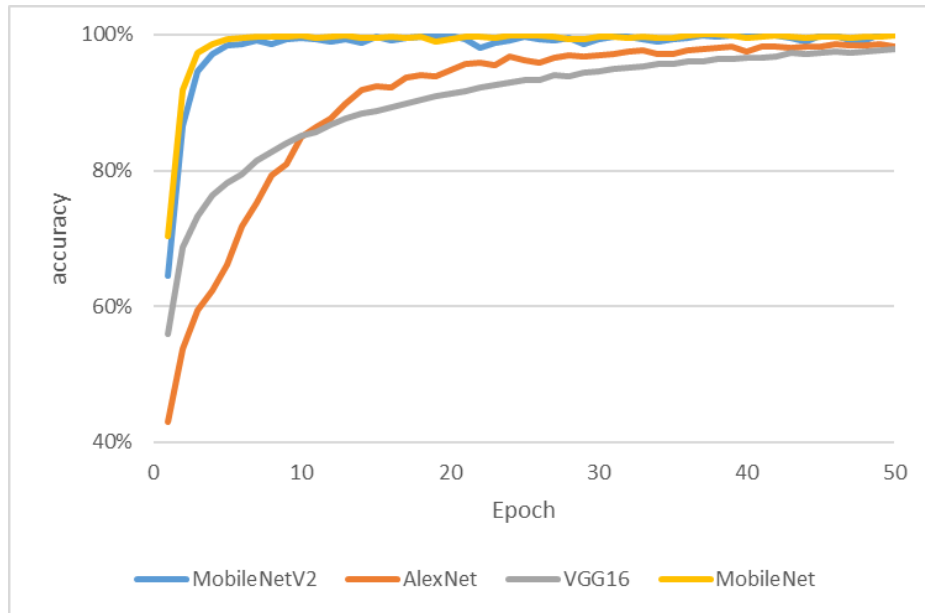
**Figure 24. Training performance for the models**

Following the training of the models, the testing data was used to assess the accuracy of the model. The overall accuracy for the 4 models is depicted in Figure 25 where it is evident that MobileNet scored the highest prediction accuracy. Also, while MobileNetv2 had a high training rate, the overall accuracy was the worst among all selected models.
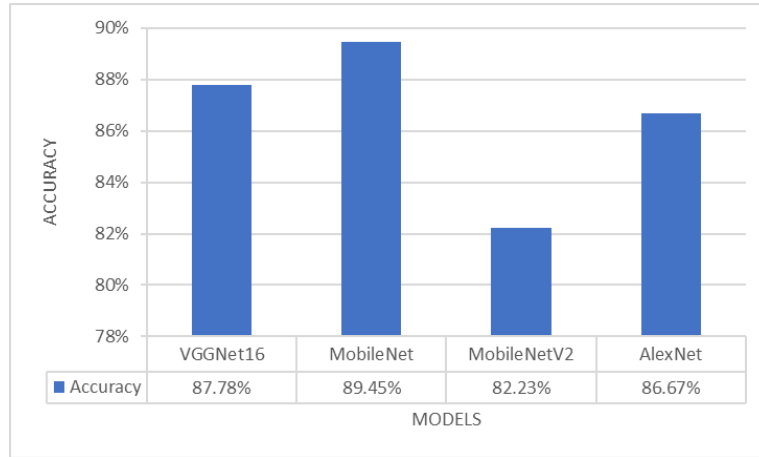
Figure 25. Test performance of the models

Furthermore, the confusion matrix for all models is shown in Figure 26. Based on the confusion matrix outcomes, MobileNet showed the highest accuracy (100%) for class HC1 with the lowest (90%) being shown by MobileNetV2 and VGGNet16. Also, MobileNet exhibited the best recognition rate (100%) for class HC2 while least (90%) being reported by both VGGNet16 and AlexNet models. Similarly, for HC3, MobileNet displayed the highest accuracy (86.7%) whereas AlexNet showed the lowest recognition rate (80%). In addition, for classes HC4, and HC5, the highest recognition rates were shown by MobileNet and VGGNet16, respectively, while the lowest recognition rates were exhibited by MobileNetV2 and AlexNet, respectively. As can be seen that the accuracies of all models for class HC5 were reduced. Finally, in the case of HC6, both MobileNetV2 and AlexNet showed the highest accuracies (90% each), whereas MobileNet displayed the least class accuracy (73.3%). Hence, it is clear that MobileNet achieved both the highest training rate and overall classification accuracy and hence it is selected to test the HC under different conditions.

37

(a)

(b)

(c)

(d)
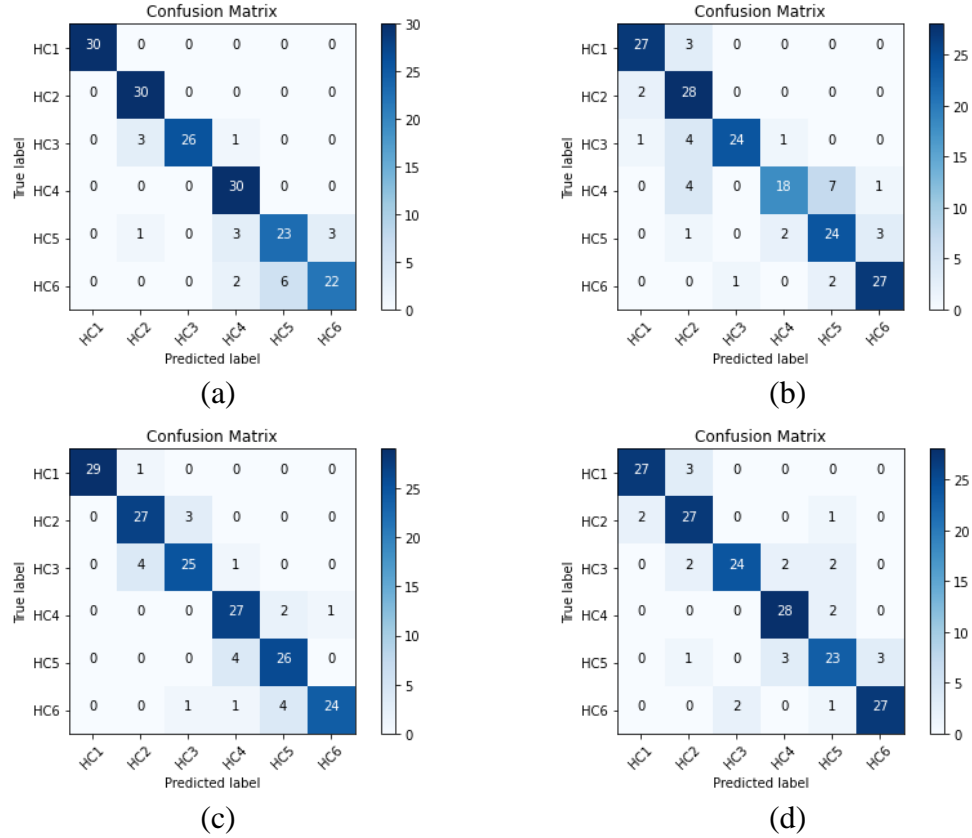
Figure 26. (a) MobileNet confusion matrix. (b) MobileNetV2 confusion matrix. (c) VGGNet16 confusion matrix. (d) AlexNet confusion matrix.

3.2 MobileNet performance under different conditions

The primary goal of this study is to propose a robust model that can detect the HC of RTV silicone rubber-coated insulators under different conditions. To accomplish this, an improvement in the accuracy of the previously discussed results under controlled indoor conditions is required. This can be achieved by reducing the number of parameters in the model, increasing the input dataset and performing image processing such as converting the dataset to the greyscale. The augmented dataset (4197 images), after image cropping, has been

utilized in the training and testing using MobileNet. Figure 27 depicts the confusion matrix results. It is evident that the classification accuracy has increased from 89.45% (when the original data was used) to 97.8%. So, increasing the dataset contributed to the increase in the classification accuracy.
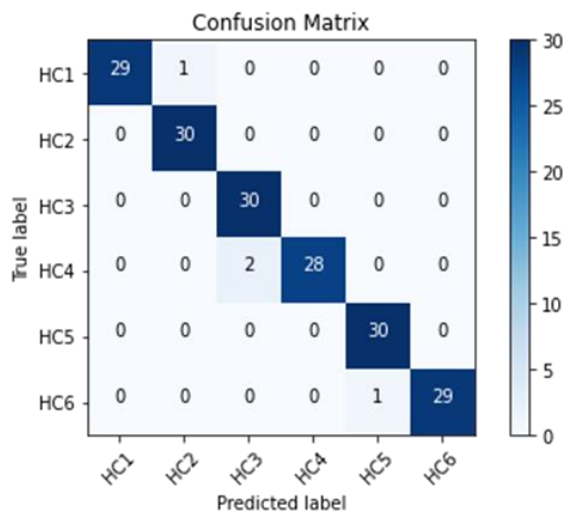
Figure 27. The indoor condition confusion matrix

It is intended to use the proposed algorithm in the field and hence one of the main challenges is to conduct the classification under different lighting conditions. So, two datasets at two different lighting conditions have been collected, i.e., bright and dark lighting conditions. Samples at both the light and dark lighting conditions are shown in Figures 28 and 29 respectively. It is worth mentioning that the samples at the different lighting conditions were used as testing samples on the original model without using any of these datasets in the training process. The overall accuracy of both the bright and dark datasets was 89.44% and 95%, respectively. Figures 30 and 31 show the confusion matrix for the test results under both

lighting conditions. It is apparent that bright lighting conditions have a more negative impact on the overall classification accuracy compared to dark lighting conditions. However, except for a few cases, all confusion between the classes happened between adjacent classes which minimize the negative impact of the class's misclassification. Authors in [44] employed the deep learning algorithm for online inspection of SIR under different lighting conditions. The model was trained based on the images taken in controlled conditions and then tested using images taken under light and dark lighting conditions which resulted in a drop in the model accuracy by around 20%. The model accuracy was improved significantly when samples taken under different lighting conditions were added to the training model. On the other hand, the drop in our model accuracy due to the change in the lighting condition was only around 8% In order to further enhance the model accuracy, 10 images taken in both bright and dark light conditions were added to the training model which resulted in increase in the overall accuracy for both the light and dark lighting conditions to 92.77% and 95.55% respectively.
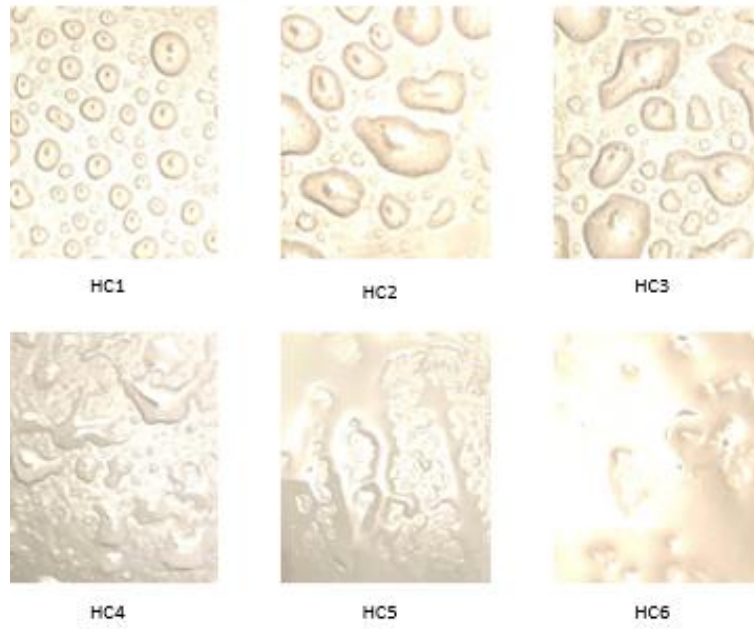
Figure 28. Samples at bright light conditions
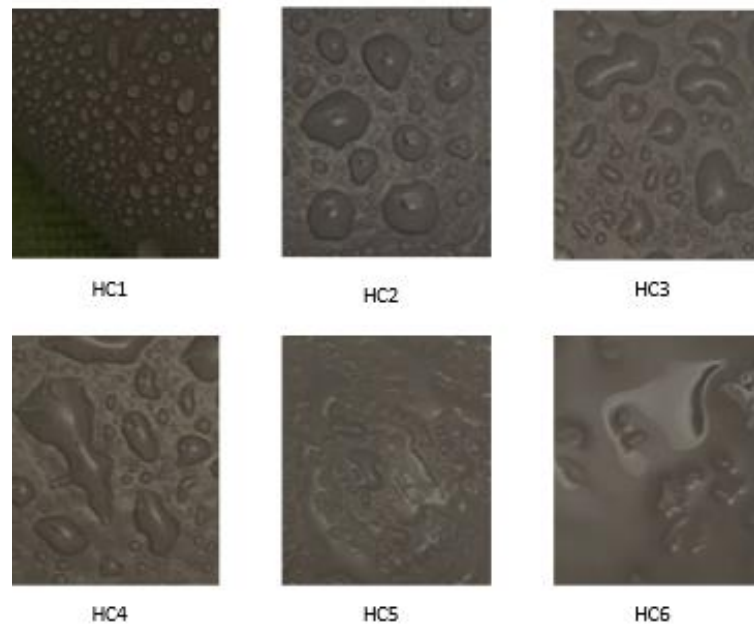
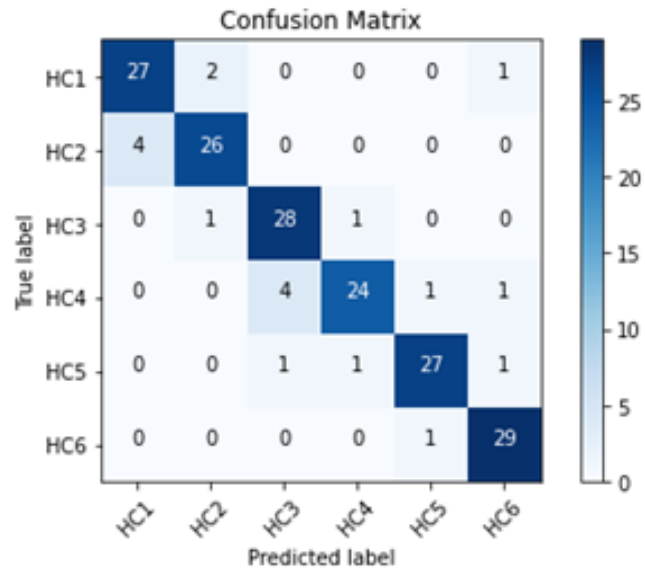

Figure 29. Samples under dark lighting conditions

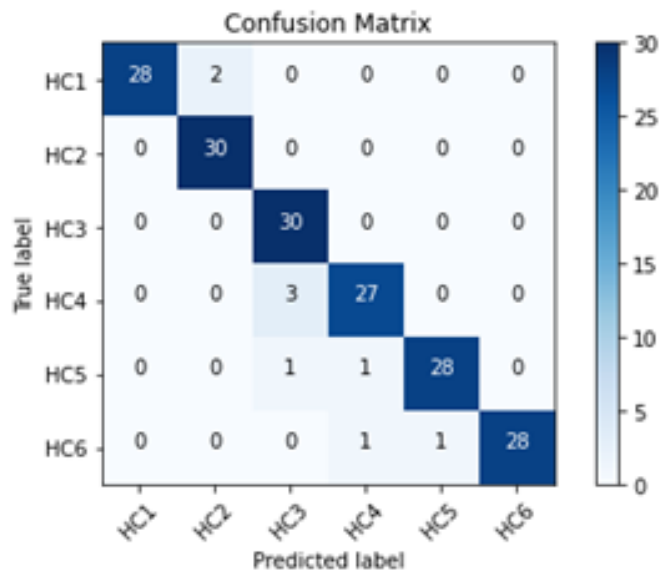**Figure 30. Confusion matrix under bright lighting conditions**

Figure 31. Confusion matrix under dark lighting conditions

	Befour training	After training
■ Bright light conditions	89.44	92.77
■ Dark light conditions	95	95.55
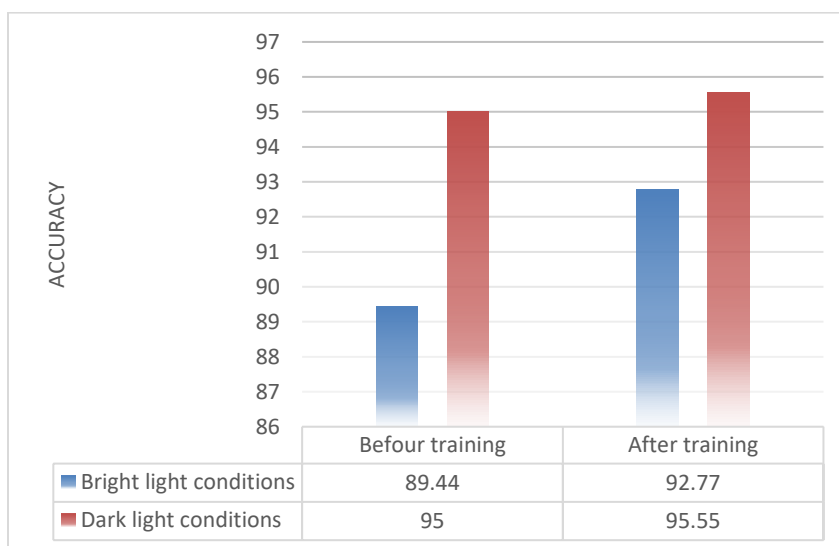
Figure 32. Comparison chart of the accuracy between before and after retraining

All previous testing of the proposed model was conducted on RTV-SIR coated insulators under various conditions. Silicone rubber can be in the form of either RTV coating or full insulators. To test the robustness of the proposed model, testing data collected from a full silicone rubber insulator has been utilized. The images were taken from the insulator sheds as shown in Figure 33. Samples of the different images with different hydrophobicity classes are shown in Figure 34. The overall accuracy of the tested data is 96.11% which is very close to the original classification accuracy. The confusion matrix is depicted in Figure 35 where it is apparent that each individual class achieved an accuracy of 90% and above. Moreover, except for one case, all misclassified cases were adjacent cases which minimize the negative impact of the misclassification.

Figure 33. A full-scale polymeric insulator
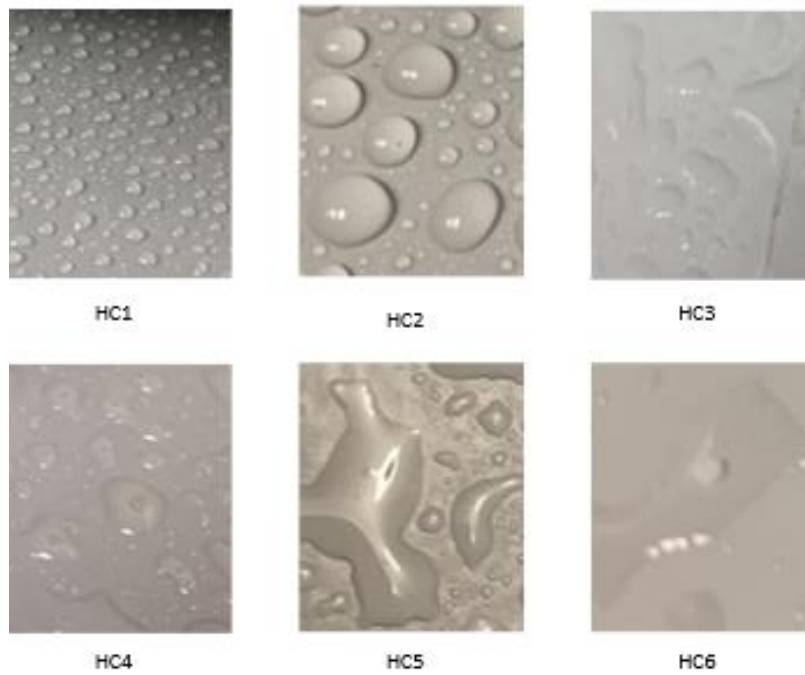
Figure 34. Samples of full insulator
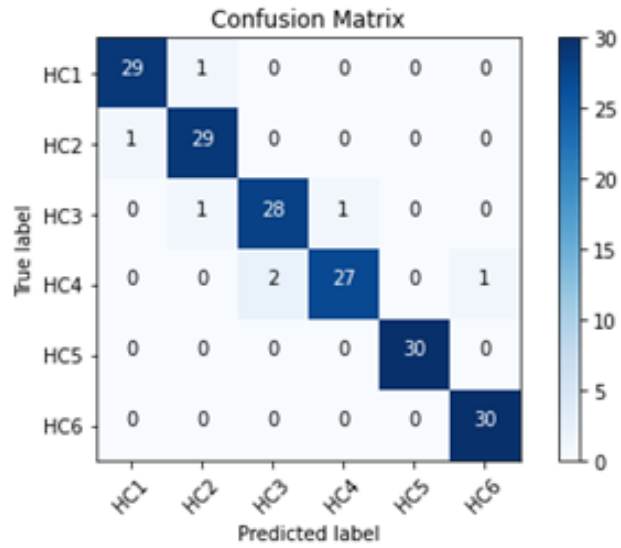
Figure 35. The confusion matrix of full insulator

Based on these findings, we can conclude that the proposed model has the ability to recognize the hydrophobicity classes (HC) in a variety of conditions, with high recognition rates without the need for additional training.

Chapter 4

CONCLUSIONS

Due to their low weight, low cost, and high hydrophobicity, silicone rubber (SIR) and room temperature vulcanized (RTV) insulators are frequently employed in transmission and distribution overhead lines as an alternative to traditional ceramic insulators. Silicone rubber-based insulating materials are preferred over conventional ceramic insulators because of their superior hydrophobicity, which prevents flashover due to deposition of contamination on their surface. Silicone rubber-based insulators are organic in nature which lead to the insulators degradation as they are subjected to electrical and environmental stresses. As the online monitoring of insulator conditions is critical, numerous electric utilities across the world have implemented several methods to assess and analyze insulator surface conditions. Most of the strategies rely on monitoring the leakage current (LC) and partial discharge (PD) activities. Other techniques, like contact angle measurements and hydrophobicity evaluation procedures, are more focused on monitoring the quality and level of aging of non-ceramic insulators. Human error is always present in the existing hydrophobicity evaluation procedures, which strongly affects the reliability of such diagnostic procedures. To overcome the human judgment aspect, some studies were proposed using digital image processing (DIP) to assess and quantify the contact angle, thereby determining the hydrophobicity class (HC) and evaluating the insulator's surface condition. Currently, there is no comprehensive online technique for assessing the class and condition of non-ceramic insulators (NCIs). Attempts have been made to construct an automatic image processing based-online system. However, these proposed

46

systems have been hampered by a variety of issues such as human intervention, localized evaluation, and specialized and set conditions.

In this thesis, an attempt is made to utilize the Convolutional Neural Networks (CNN), Transfer Learning (TL), and Object Detection (OD) to categorize and assess the hydrophobicity classes (HC) of silicone rubber insulator material. For the training purpose, a dataset of classes 1–6 includes a total of 4197 images that were cropped and resized to (224×224 pixels) was collected. The MobileNet model has been trained under controlled indoor and tested in different conditions, including indoor, bright lighting, and dark lighting conditions, resulting in an accuracy of 97.77 percent, 89.44 percent, and 95 percent, respectively. Furthermore, the proposed model was tested on a full-scale silicone rubber insulator and achieved a recognition rate of 96.11 percent. The proposed model was developed and deployed as a web application to increase the usability of the project. The goal of this thesis is to create a robust deep learning based classification system that can evaluate the condition of SIR insulators under several conditions. The proposed method is intended to decrease the cost and effort associated with the traditional human-based examination. While the proposed model achieves very high recognition rates in all tests, it can be improved further by retraining the model with more images in different conditions including addition of pollution, different insulators colors and profiles.

References

[1] C. Bayliss and B. Hardy, Transmission and Distribution Electrical Engineering, Third Edition, 2007, Elsevier Ltd.

[2] F. Alhebshi, H. Alnabilsi, J. Alzebaidi, A. Bensenouci, T. Brahimi and M. Bensenouci, "Monitoring the operation of transmission line in a smart grid system through IoT," 2018 15th Learning and Technology Conference (L&T), 2018, pp. 139-146, doi: 10.1109/LT.2018.8368498.

[3] I. Jarrar, Feasibility Study: "To implement unmanned aviation vehicles to inspect and scan (infrared) the electrical network (HV Cables, OH Lines, LV systems) and water pipelines," ASTRO Initiative Cards-Transco 14, October 2011.

[4] I.Jarrar, A. El Hag and N. Qaddoumi, "Online techniques to detect defects in Non-Ceramic Insulators (NCI)," GCC Cigre, Doha, Qatar, Nov-2010.

[5] A. El Hag, "Effect of Insulator Profile on Ageing Performance of Silicone Rubber Insulators", Ph.D. dissertation, Dept. Elect. Eng, Waterloo University, 2003

[6] M. S. Naidu and V. Kamaraju, High Voltage Engineering, Second Edition, 1995, Tata McGraw-Hill Publishing Ltd.

[7] Siderakis, K., Pylarinos, D., Thalassinakis, E., Vitellas, I., & Pyrgioti, E. (2011). Pollution maintenance techniques in coastal high voltage installations. Engineering, Technology & Applied Science Research, 1(1), 1-7.

[8] A. El Hag, High Voltage Engineering lecture notes. [On-line], Available: https://ilearn.aus.edu/webapps/portal/frameset

[9] J.L. Goudie, M. J. Owen, and T. Orbeck. "A review of possible degradation mechanisms of silicone elastomers in high voltage insulation applications." In Electrical Insulation and Dielectric Phenomena, 1998. Annual Report. Conference on, vol. 1, pp. 120-127. IEEE, 1998.

[10] High Voltage Silicone Insulators, Electricity Power Technology of the Future, Elkom-NET ltd, Skopje, Macedonia, Product Catalog, June 2009.

[11] M. Amin and M. Salman, "Ageing of Polymeric Insulators (An Overview)," Advanced Study Center. Rev.Adv.Mater.Sci. Vol. 13, pp 93-116, 2006.

[12] Electric Field Computation, HVEL, High Voltage Engineering Laboratory. [On-line] Retrieved from: http://www.power.uwaterloo.ca/HVEL/Research-_Electricfield.htm.

[13] M. Amin, M. Akbar and S. Amin, "Hydrophobicity of Silicone Rubber Used for Outdoor Insulation (An Overview)", Advanced Study Center Co. Ltd, Pakistan Taxila, Rev.Adv.Mater.Sci. 16 (2007) 10-26, 2007.

[14] N. Yoshimura, S. Kumagai and S. Nishimura, "Electrical and environmental aging of silicone rubber used in outdoor insulation," in IEEE Transactions on Dielectrics and Electrical Insulation, vol. 6, no. 5, pp. 632-650, Dec. 1999, doi: 10.1109/TDEI.1999.9286756.

[15] Souza, A. L., & Lopes, I. J. (2006, June). Electric field distribution along the surface of high voltage polymer insulators and its changes under service conditions. In Conference Record of the 2006 IEEE International Symposium on Electrical Insulation (pp. 56-59). IEEE.

[16] S. Gubanski et al, "Tracking on Insulator Surfaces in Presence of Conductive Defects within Housing to Core Interface," INMR World Congress, Issue 84 Quarter Two 2009 Volume 17 Number 2 Page 74.

[17] Using Infrared Thermography in Utilities, FLIR. [On-line] Retrieved from: http://www.flir.com/thermography/eurasia/en/content/?id=11430.

[18] I. Jarrar, H. Bashiri, and M. Kuheel, "Partial discharge detection techniques," Department of Electrical Engineering, B.S. design project, American University of Sharjah, UAE, 2008.

[19] M. Muhr, R. Schwarz, S. Pack and B. Koerbler, "Unconventional partial discharge measurement," Annual Report Conference on Electrical Insulation and Dielectric Phenomena, 2004.

[20] STRI Guide: "Composite Insulator Status Program: Field inspection of composite insulators", Guide 3, 98/1, 1998.

[21] Z. Linjie et al, "On-line hydrophobicity measurement of composite insulators," School of Electrical Engineering, North China Electric Power University, Beijing, 102206, P.R.China.

[22] Y. Liu et al, "A New Diagnosis Method on Insulators with Measuring Contact Angles," International Journal of Intelligent Engineering and Systems, School of Electronic Information, Wuhan University, P.R. China, Vol.2, No.2,2009.

[23] B. X. Du and Yong Liu, "Pattern Analysis of Discharge Characteristics for Hydrophobicity Evaluation of Polymer Insulator," IEEE Transactions on Dielectrics and Electrical Insulation, Vol. 18, No. 1; February 2011.

[24] M. Berg, R. Thottappillil and V. Scuka, "Hydrophobicity Estimation of HV Polymeric Insulating Materials: Development of a Digital Image Processing Method," IEEE Transactions on Dielectrics and Electrical Insulation, Vol. 8 No. 6, December 2001.

[25] D. Thomazini, M. V. Gelfuso and R. Altafim, "Hydrophobicity Classification of Polymeric Materials Based on Fractal Dimension," Materials Research, Vol. 11, No. 4, 415-419, 2008

[26] T. Tokoro, Y. Omoto, Y. Katayama and M. Kosaki, "Image analysis of hydrophobicity and dielectric property of polymer insulating material," IEEE 2002 Annual Report Conference on Electrical Insulation and Dielectric Phenomena.

[27] S. Yi, L. Qin, T. Liangrui and Y. Qiuxia, "A Detection Algorithm of Hydrophobic Levels Based on Triangle Module Operator," Electrical and Electronic Engineering School in North China Electric Power University, Beijing, China.

[28] Y. Sun, Q. Li, L. Tang and Q. Yang, "The Fusion Estimating Algorithm of Hydrophobic Level Based on D-S Evidence Theory," School of Electrical and Electronic Engineering, North China Electric Power University, Beijing, China.

[29] I. Jarrar, K. Assaleh and A. H. El-hag, "Using a pattern recognition-based technique to assess the hydrophobicity class of silicone rubber materials," in IEEE Transactions on Dielectrics and Electrical Insulation, vol. 21, no. 6, pp. 2611-2618, December 2014, doi: 10.1109/TDEI.2014.004523.

[30] Sun, Q., Lin, F., Yan, W., Wang, F., Chen, S., & Zhong, L. (2018). Estimation of the hydrophobicity of a composite insulator based on an improved probabilistic neural network. Energies, 11(9), 2459.

[31] Q. Wang et al., "The hydrophobic detection of transformer composite insulator bushing based on digital image processing technique," 2016 IEEE International Conference on High Voltage Engineering and Application (ICHVE), 2016, pp. 1-4, doi: 10.1109/ICHVE.2016.7800844.

[32] Q. Wang et al., "The Study of the Improved Multilayer Perceptron Algorithm on Hydrophobicity Detection Research of Composite Insulator Bushing," 2016 8th International

Conference on Intelligent Human-Machine Systems and Cybernetics (IHMSC), 2016, pp. 438-441, doi: 10.1109/IHMSC.2016.265.

[33] Yang, L., Bi, J., Hao, Y., Nian, L., Zhou, Z., Li, L., ... & Zhang, F. (2018). A recognition method of the hydrophobicity class of composite insulators based on features optimization and experimental verification. Energies, 11(4), 765.

[34] Jayabal, R., Vijayarekha, K., & Rakesh Kumar, S. (2018). Design of ANFIS for hydrophobicity classification of polymeric insulators with two-stage feature reduction technique and its field deployment. Energies, 11(12), 3391.

[35] Y. Fahmy and A. El-Hag, "Application of Convolution Neural Network in Hydrophobicity Classification," 2021 IEEE Electrical Insulation Conference (EIC), 2021, pp. 490-493, doi: 10.1109/EIC49891.2021.9612318.

[36] Kokalis, C. C. A., Tasakos, T., Kontargyri, V. T., Siolas, G., & Gonos, I. F. (2020). Hydrophobicity classification of composite insulators based on convolutional neural networks. Engineering Applications of Artificial Intelligence, 91, 103613.

[37] Chatterjee, S., Roy, S. S., Samanta, K., & Modak, S. (2020). Sensing wettability condition of insulation surface employing convolutional neural network. IEEE Sensors Letters, 4(7), 1-4.

[38] Krizhevsky, Alex, Ilya Sutskever, and Geoffrey E. Hinton. "Imagenet classification with deep convolutional neural networks." Advances in neural information processing systems 25 (2012).

[39] Alom, M. Z., Taha, T. M., Yakopcic, C., Westberg, S., Sidike, P., Nasrin, M. S., ... & Asari, V. K. (2019). A state-of-the-art survey on deep learning theory and architectures. Electronics, 8(3), 292.

[40] Howard, A. G., Zhu, M., Chen, B., Kalenichenko, D., Wang, W., Weyand, T., ... & Adam, H. (2017). Mobilenets: Efficient convolutional neural networks for mobile vision applications. arXiv preprint arXiv:1704.04861.

[41] Junejo, I. N., & Ahmed, N. (2021). Depthwise separable convolutional neural networks for pedestrian attribute recognition. SN Computer Science, 2(2), 1-11.

[42] Yosinski, J., Clune, J., Bengio, Y., & Lipson, H. (2014). How transferable are features in deep neural networks? arXiv preprint arXiv:1411.1792.

[43] Liu, W., Anguelov, D., Erhan, D., Szegedy, C., Reed, S., Fu, C. Y., & Berg, A. C. (2016, October). Ssd: Single shot multibox detector. In European conference on computer vision (pp. 21-37). Springer,

[44] El Haj, Y., El-Hag, A. H., & Ghunem, R. A. (2021). Application of deep-learning via transfer learning to evaluate silicone rubber material surface erosion. IEEE Transactions on Dielectrics and Electrical Insulation, 28(4), 1465-14.